European Journal of Pharmacology 994 (2025) 177314

Contents lists available at ScienceDirect

European Journal of Pharmacology

journal homepage: www.elsevier.com/locate/ejphar

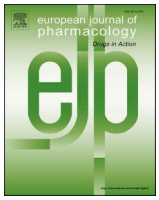

Octreotide attenuates experimental severe acute pancreatitis through inhibiting pyroptosis and modulating intestinal homeostasis

Mengqi Zhao [a,b], Mengyan Cui [a,b], Miaoyan Fan [a,b], Chunlan Huang [b], Jingjing Wang [a], Yue Zeng [b], Xingpeng Wang [b,**], Yingying Lu [b,*]

[a] Shanghai Key Laboratory of Pancreatic Disease, Shanghai Jiaotong University School of Medicine, Shanghai, 201620, China
[b] Department of Gastroenterology, Shanghai General Hospital, Shanghai Jiaotong University School of Medicine, Shanghai, 201620, China

ARTICLE INFO

Keywords:
Octreotide
Acute pancreatitis
Intestinal microbiota
Pyroptosis
Intestinal barrier

ABSTRACT

Severe acute pancreatitis (SAP) is a common clinical condition characterized by acute abdominal symptoms. Octreotide (OCT) is a commonly prescribed treatment for acute pancreatitis (AP). Recent research shows that pyroptosis and intestinal homeostasis significantly contribute to the progression of AP. However, it remains unclear whether OCT treats SAP through modulating pyroptosis and intestinal microbiota. Our study aimed to investigate and validate the potential therapeutic effects of OCT on SAP and underlying mechanisms. The inhibition of pyroptosis in mice using disulfiram was investigated to elucidate the role of pyroptosis in AP. Molecular biology experiments confirmed that OCT effectively inhibited the expression of pyroptosis-related markers. Additionally, the composition, abundance, and functionality of the intestinal microbiota were analyzed using 16S rRNA sequencing, while short-chain fatty acids (SCFAs) were quantified by targeted metabolomics. Our study demonstrated that the administration of OCT significantly mitigated the severity of SAP in a dose-dependent manner. Furthermore, the inhibition of pyroptosis in mice attenuated SAP, thereby highlighting the critical role of pyroptosis in this condition. OCT administration was observed to suppress the expression of key pyroptosis markers. Additionally, there was a notable reduction in intestinal permeability and bacterial translocation. OCT reverses gut dysbiosis caused by SAP, increasing beneficial bacteria while inhibiting pathogenic strains. Furthermore, OCT administration enhanced the levels of SCFAs, including propanoic acid, acetic acid, and butyric acid. Our findings indicate OCT has the potential to alleviate SAP by suppressing pyroptosis and restoring intestinal homeostasis.

1. Introduction

Acute pancreatitis (AP) is a severe inflammatory condition distinguished by its abrupt onset and swift advancement, often leading to a high rate of mortality (Petrov and Yadav, 2019). Approximately 20% of individuals affected by this disease progress develop severe acute pancreatitis (SAP), marked by pancreatic necrosis, infection, and multi-organ failure, resulting in mortality rates ranging from 15 to 35% (Barreto et al., 2021; Schepers et al., 2019). Despite advancements in understanding the pathogenesis of AP, gaps in knowledge persist, necessitating further investigation for effective treatment strategies. Recent research has highlighted the role of pyroptosis, a type of programmed cell death, in the evolution and aggravation of AP (Fan et al., 2021; Gao et al., 2021). Pyroptosis can exacerbate pancreatic tissue damage and trigger the onset of systemic inflammatory response syndromes, which has an impact on the progression and prognosis of the disease. The caspase-1-dependent classical inflammasome pathway and the caspase-4/5/11-dependent nonclassical inflammasome pathway play roles in pyroptosis. Pyroptosis, in addition to its function in eliminating intracellular infections, can release an excessive quantity of inflammatory cytokines, potentially exacerbating the pathological state.

The intestine is particularly vulnerable and frequently serves as the principal target in the pathogenesis of AP (Liu et al., 2022a). Emerging research findings suggest a dysbiosis of the intestinal microbiota, impairment of the intestinal barrier, and dysfunction of the immune system in cases of AP (Li et al., 2020; Zou et al., 2022a). Disruption of intestinal homeostasis may lead to the translocation of intestinal bacteria, further exacerbating the condition of AP (Liu et al., 2019). Given

* Corresponding author.
** Corresponding author.
E-mail addresses: richardwangxp@163.com (X. Wang), le_voyageur@sjtu.edu.cn (Y. Lu).

https://doi.org/10.1016/j.ejphar.2025.177314
Received 13 October 2024; Received in revised form 23 January 2025; Accepted 24 January 2025
Available online 6 February 2025

the significant impact of gut function on the progression of AP, maintaining the integrity of the intestinal barrier has emerged as a crucial objective in the management of SAP (Yan et al., 2023).

Octreotide (OCT) is a frequently employed somatostatin analog in clinical settings, distinguished by its prolonged duration of action and notable therapeutic effectiveness (Zhang et al., 2024). Its applications extend to the management of AP and prophylaxis against post-endoscopic retrograde cholangiopancreatography (ERCP) pancreatitis (Li et al., 2007). In addition to its inhibitory effects on pancreatic enzyme release, OCT has been shown to mitigate inflammatory damage by modulating signaling cascades (Borzsei et al., 2023). Despite its broad therapeutic utility (La Salvia et al., 2023; Xu et al., 2022; Zou et al., 2022b), the impact of OCT administration on the pancreatic acinar cells and intestinal microbiota remains uncertain. The exact mechanism of the therapeutic effect of OCT in acute pancreatitis remains to be elucidated.

Here, we aimed to develop a deeper understanding of the underlying mechanisms of the roles of OCT in SAP management.

2. Materials and methods

2.1. Animals

Male C57BL/6 mice (6–8 weeks, 20–22 g) were obtained from Shanghai Anduo biotechnology Co., Ltd. (Shanghai, China; license number: SYXK (Hu) 2024-0012) and kept under specific pathogen-free (SPF) conditions. The specific feeding environment was as follows: temperature of 23 ± 2 °C, relative humidity of 40–60%, free access to water and mouse chow and lighting source with a 12-h shift of the light-dark cycle. All the animal experiments were approved by the Institutional Animal Care and Use Committee (IACUC) of Shanghai General Hospital Affiliated to Shanghai Jiao Tong University School of Medicine (2022AWS0027) and conducted according to the instructions of the IACUC.

2.2. Experimental design

In this study, two additional types of acute pancreatitis (AP) murine models were established. For the L-arginine-induced SAP model, mice were administered 8% L-arginine (Sigma-Aldrich, USA) at a dosage of 4 g/kg intraperitoneally, with two injections given 1 h apart. Mice were sacrificed 72 h after the initial L-arginine injection (Dawra et al., 2007). In the caerulein + LPS-induced SAP model, mice received caerulein (MedChemExpress, China) at a dosage of 100 μg/kg (Lerch and Gorelick, 2013) intraperitoneally for a total of 10 injections, with a 1-h interval between each injection. Lipopolysaccharide (LPS) (Sigma-Aldrich, USA) at a dosage of 5 mg/kg was administered intraperitoneally immediately after the final caerulein injection. Mice were sacrificed 12 h after the initial caerulein injection (Fig. S1ab).

In the disulfiram study, mice were divided into the Con group, the SAP group and the DSF group. The SAP group was established by L-arginine induced. The DSF group was established by injecting 100 mg/kg disulfiram (MedChemExpress, China) per day after inducing SAP of L-arginine-induced (Fig. S1c). Mice were sacrificed 72 h after the initial L-arginine injection. According to the dosage suggested in previous studies (Zhao et al., 2022). In the OCT study, mice were divided into the Con group, the SAP group, the OCT10 group, the OCT50 group and the OCT100 group. Octreotide (Topscience, China) was administered at concentrations of 10 μg/kg, 50 μg/kg, and 100 μg/kg, respectively. According to the dosage suggested in previous studies (El-Sisi et al., 2021; Mohamed et al., 2021). In the Ulinastatin study, mice were divided into the Con group, the SAP group, the OCT100 group, and the ULI group. Ulinastatin (MedChemExpress, China) was administered at concentrations of 1000 U/kg. All three OCT groups were injected with the appropriate concentration of OCT after each injection of L-arginine or caerulein (Fig. S1ab).

2.3. Histological analysis

Fresh pancreas, ileum, and lung specimens underwent fixation with 4% paraformaldehyde, dehydration, and paraffin embedding. Thin sections (4-μm thick) were prepared, stained with hematoxylin and eosin (H&E), and then observed under a light microscope (Leica, Germany) at magnifications of × 100 or × 200 to assess morphologic changes. The histopathological alterations in the pancreas, specifically pancreatic edema, acinar cell necrosis, and inflammation, were graded based on the criteria established by Schmidt (Shimizu et al., 2000). Similarly, pathological lesions in the ileum, such as mucosal damage, inflammation, and congestion, were scored according to Chiu's standard (Banks et al., 2013). Pathologic injuries of the lung tissue were referred to the Smith scoring system and included pulmonary edema, alveolar and interstitial inflammation, pulmonary atelectasis, and hyaline membrane formation (Smith et al., 1997).

2.4. Serum amylase and lipase assay

According to the technicians' instructions, the Advia 2400 chemistry system (Siemens, German) was used to measure the serum amylase activity using amylase reagents. Serum activity of lipase was detected using assay kits (Jiancheng Biotech, Nanjing, China). All kits were used according to the manufacturer's instructions.

2.5. Enzyme-linked immunosorbent assay (ELISA)

The serum and pancreas levels of IL-1β, IL-6, and TNF-α were assayed (MultiSciences Lianke Biotech Co., Ltd., China) in accordance with the manufacturer's guidelines. Similarly, myeloperoxidase (MPO) was detected using designated kits (Nanjing Jiancheng Bioengineering Institute, China) as per the manufacturers' instructions.

2.6. Quantitative Real-time PCR

The inflammatory cytokines and the pyroptosis-associated cytokines were quantified by real-time PCR. Reverse transcription (RT) was conducted using HyperScript III RT SuperMix for qPCR in conjunction with the gDNA Remover Kit (both from EnzyArtisan, Shanghai, China). All primers, which were custom-synthesized by EnzyArtisan (China), are listed in Table S1. Real-time PCR was performed with 2xS6 Universal SYBR qPCR Mix (EnzyArtisan, Shanghai, China), adhering strictly to the manufacturer's guidelines. The relative expression levels of the genes were determined using the 2-ΔΔCt method.

2.7. PAC isolation and culture

Pancreatic acinar cells (PACs) from C57BL/6 mice were isolated using a collagenase digestion method, which included the extraction of the pancreas, digestion with collagenase at 37 °C, dispersion by pipetting, and filtration through a nylon mesh cloth. The isolated acinar cells were then cultured at 37 °C in Dulbecco's modified Eagle's medium/Ham F-12 medium (DMEM-F12) supplemented with 10% fetal bovine serum (FBS) for subsequent experimental treatments. Both DMEM-F12 and FBS were obtained from Bioagrio, china.

2.8. Cell viability assay

The effects of LPS and OCT on the cell viability of PACs were measured using CCK8 (Topscience, China) according to the manufacturer's instructions. PACs were incubated at 1 ng/ml LPS (Sigma-Aldrich, USA) and different concentrations of OCT (0 nM, 0.1 nM, 1 nM, 10 nM, 100 nM, 1000 nM, 10,000 nM) for 6 h. Then 10 μl CCK-8 reagent was added to the cells, followed by another 2 h of incubation. Finally, the absorbance at 450 nm was measured.

2.9. LDH activity assay

After stimulation with 1 ng/ml LPS, acini were separated through centrifugation, and the resulting cell-free supernatant was employed to assess lactate dehydrogenase (LDH) activity levels. This was achieved using a mice LDH ELISA kit (Beyotime Biotechnology, China), following the manufacturer's guidelines. Finally, the absorbance at 490 nm was measured.

2.10. Immunofluorescence

Pancreatic and ileal paraffin sections underwent dewaxing, and antigens were recovered using a citric acid buffer (Sangon Biotech, China). After repeated rinsing in phosphate-buffered saline (PBS), a circular outline was delineated around the tissue using a super pap pen (Sangon Biotech, China). Following this, the slides were blocked with a blocking buffer (Sangon Biotech, China) for 1 h at room temperature. The slides were then incubated with primary antibodies against IL-1β (catalog number 12507; Cell Signaling Technology, USA), HMGB1 (catalog number A25444; Abclonal, China), GSDMD (catalog number A20728; Abclonal, China), ASC (catalog number A11433; Abclonal, China), occludin (catalog number A2601; Abclonal, China), claudin1 (catalog number A21971; Abclonal, China) and ZO-1 (catalog number A0659; Abclonal, China) diluted with primary antibody dilution buffer (Sangon Biotech, China) at 4 °C overnight. Subsequently, the slides were cleaned with PBS and incubated with fluorescein-labeled secondary antibodies (Yeason, China) for 1 h in a dark environment before being stained with dihydrochloride (DAPI) for 5 min to visualize the nucleus. Images were captured using a fluorescence microscope (Leica, USA).

2.11. TUNEL staining

Apoptotic cell death in the pancreas was assessed through a TUNEL assay, utilizing a fluorescein TUNEL cell apoptosis detection kit (Beyotime Biotechnology, China) in accordance with the manufacturer's guidelines. The counting of TUNEL-positive cells in the pancreas was conducted at 200 × magnification.

2.12. FISH

Fluorescence in situ hybridization (FISH) was used to detect bacterial translocation. Briefly, paraffin sections of the pancreas and ileum underwent dewaxing, antigen retrieval, and digestion with Proteinase K for 20 min at 37 °C. The sections were pre-hybridized at 37 °C for 1 h, followed by overnight incubation with specific probes (EUB338 [5′-Cy3-GCTGCCTCCCGTAGGAGT-3']) in a humidified chamber. Subsequently, the sections were washed and stained with 49,6-diamidino-2-phenylindole (DAPI). Images were captured using a fluorescence microscope (Leica, Nussloch, Germany).

2.13. Antibiotic treatment

Enteric germ-free mice were created by administering an antibiotic cocktail mixture for a duration of four weeks. The cocktail consisted of the following antibiotics: ampicillin (1 g/l, sourced from Sangon, China), vancomycin (0.5 g/l, Sangon, China), neomycin (1 g/l, Sangon, China), and metronidazole (1 g/l, also from Sangon, China).

2.14. Fecal microbiota transplantation

The methodology involved the collection of feces from Con mice, OCT mice, SAP mice, and OCT + SAP mice for fecal microbiota transplantation (FMT). SAP models were established by caerulein and LPS. The OCT dosage for the OCT group is identical to that of the OCT100 group. The FMT suspension was prepared within a time frame of less than 2 h, with 100 mg of feces resuspended in 1 mL of saline and subsequently centrifuged for 5 min to obtain the suspension for transplantation. The suspension was administered to enteric germ-free mice by gavage. Mice were divided into four groups: the FMT-Con group, the FMT-OCT group, the FMT-SAP group, and the FMT-OCT + SAP group. The FMT-Con group was gavaged with 200 μL of an FMT suspension from Con mice for 1 week, the FMT-OCT group was gavaged with 200 μL of an FMT suspension from OCT mice for 1 week, the FMT-SAP group was gavaged with 200 μL of an FMT suspension from SAP mice for 1 week and the FMT-OCT + SAP group was gavaged with 200 μL of an FMT suspension from OCT + SAP mice for 1 week. SAP is subsequently induced by the caerulein + LPS-induced SAP model.

2.15. Gut microbiota analysis

Genomic DNA was isolated from the microbial population of cecum luminal contents and feces samples using the Magnetic Soil And Stool DNA Kit, following the manufacturer's instructions. High-throughput sequencing was subsequently performed on the Majorbio Cloud platform.

2.16. Short-chain fatty acids (SCFAs) analysis

Fecal samples were collected and stored at −80 °C for analysis. The fecal supernatant was prepared for examination by extracting it with a mixture of internal standards, including 2-ethylbutyric acid obtained from Sigma-Aldrich and methanol. The levels of propanoic acid, acetic acid, and butyric acid were then quantified using a GC–MS system from Agilent Technologies. Reference standards for short-chain fatty acids (SCFAs) were acquired from Merck (Darmstadt, Germany).

2.17. Statistics

All measured data were expressed as mean ± SEM and analysis was performed using GraphPad prism 8.0 software. The Student's t-test was used to compare the two groups. For the comparison of more than two groups, the one-way analysis of variance (ANOVA) was performed. For data that did not correspond to the normal distribution, the Kruskal-Wallis test was used. Differences were classified as statistically significant at $p < 0.05$.

3. Results

3.1. Inhibition of pyroptosis reduces the severity of SAP

In order to investigate the potential role of pyroptosis in AP, we employed L-arginine-induced SAP mouse models and administered disulfiram, a recognized inhibitor of pyroptosis that blocks GSDMD pore formation. Immunofluorescence staining for IL-1β and HMGB1 further confirmed the inhibitory effect of disulfiram on pyroptosis (Fig. 1a and b). The inhibition of pyroptosis correlated with a significant reduction in pancreatic pathological damage, serum amylase and lipase levels in the disulfiram-treated group compared to the SAP group (Fig. 1c and d). In addition, disulfiram effectively reduced the levels of inflammatory cytokines TNF-α, IL-1β and IL-6 in both serum and pancreas tissues, as well as myeloperoxidase (MPO) levels in the pancreas (Fig. 1e–g). Pathological examination of lung and ileum tissues indicated injury and inflammatory markers, suggesting inhibition of the pyroptosis response in mice attenuated the damage to distant organs during AP (Figs. S1d–g). In summary, our findings demonstrate that inhibition of pyroptosis markedly alleviates the severity of SAP.

3.2. OCT treatment reduces the severity of SAP both in vivo and in vitro

The current results exhibit the therapeutic effects of various OCT concentrations on L-arginine-induced experimental SAP. Histological evaluations indicated that different OCT dosages produce unique

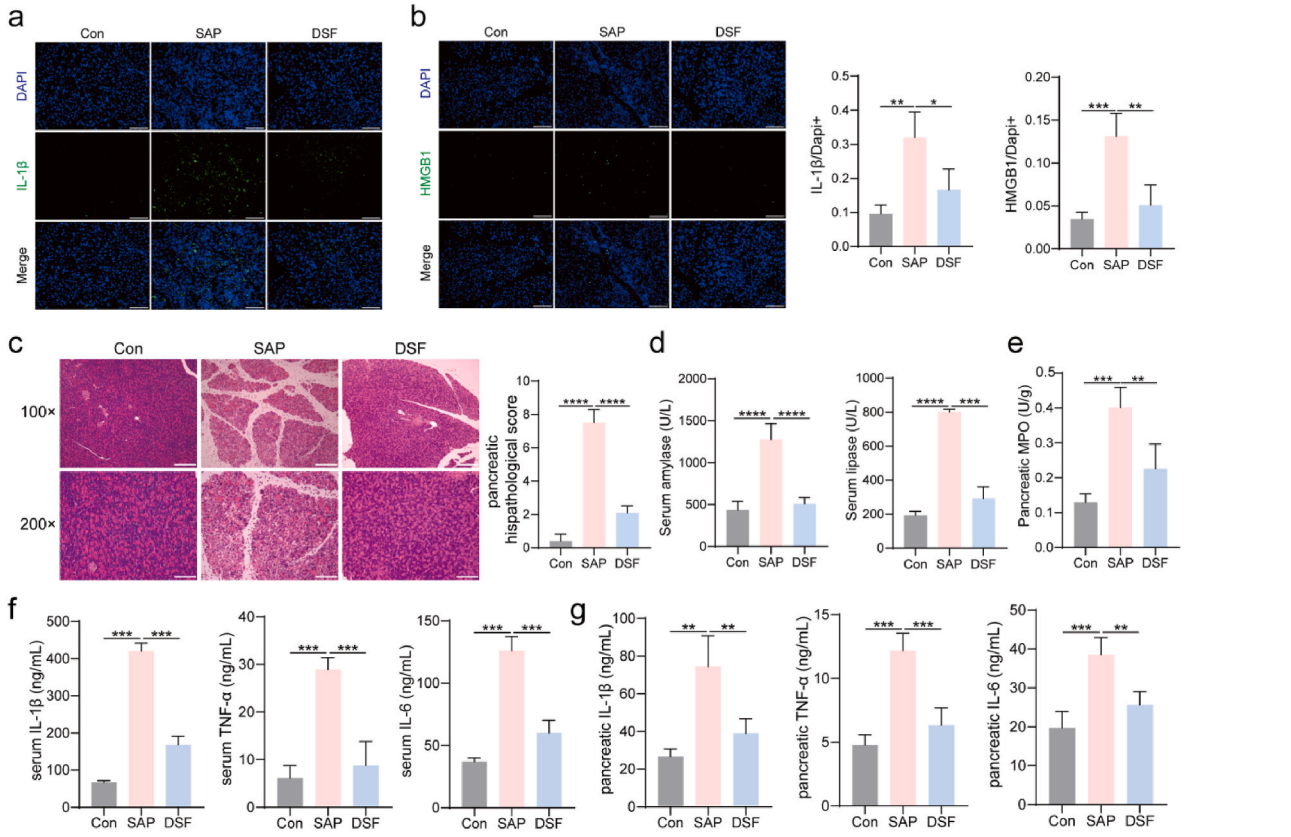

Fig. 1. Inhibition of pyroptosis alleviated SAP. (a, b) Immunofluorescence staining and quantification of IL-1β and HMGB1 in the pancreas (200 × magnification) (n = 5 mice per group). **(c)** Histopathological changes of pancreas samples observed by HE staining. Original magnification, 100 × (the upper figures) or 200 × (the lower figures). (n = 5 mice per group) **(d)** The level of serum amylase and lipase. **(e)** The pancreatic level of MPO. **(f)** Serum levels of IL-1β, TNF-α and IL-6. **(g)** Pancreatic levels of IL-1β, TNF-α and IL-6. The symbol *means $P < 0.05$, **means $P < 0.01$, ***means $P < 0.001$ and ns means $P > 0.05$.

therapeutic outcomes. As shown in Fig. 2a, OCT caused dose-dependent histopathological improvements in pancreatic tissue histopathology, including reduced edema, necrosis and inflammatory infiltration. Notably, although there was no statistically meaningful difference in histology scores between the SAP group and the OCT10 group, the OCT50 and OCT100 groups significantly lowered total histologic scores compared to the SAP group. Furthermore, OCT dramatically and dose-dependently decreased MPO levels in pancreatic tissue (Fig. 2c). Likewise, the administration of OCT resulted in a dose-dependent decrease in serum amylase and lipase levels and inflammatory markers, including TNF-α, IL-1β and IL-6 (Fig. 2b–d). Ulinastatin lessens pancreatic injury in SAP, but OCT100 is more effective (Fig. S2a). It also partially lowers molecules linked to pyroptosis, though their levels remain higher compared to OCT100 (Fig. S2b).

To confirm the aforementioned findings, we conducted in vitro studies. Initially, the expression levels of pyroptosis markers and inflammatory factors were assessed at different time intervals (3h, 6h and 9h) (Fig. S2c). The peak expression was observed at the 6-h time point, leading to select it as the experimental time point. The cytotoxicity of OCT in PAC was assessed using Cell Counting Kit-8 (CCK-8) at concentrations ranging from 0.1 nM to 10,000 nM. Our results indicated that OCT had negligible effects on cell viability, prompting us to narrow down the experimental concentration range to 0.1–100 nM (Fig. S2d). In PAC treated with LPS and varying concentrations of OCT (0.1–100 nM), we observed similar trends in cytotoxicity as in the in vivo experiments using the CCK-8 assay (Fig. S2e). In addition, our results indicated a significant decrease in cellular LDH activity in the supernatant, indicating reduced cell damage in the presence of 0.1–100 nM OCT (Fig. S2f).

In summary, both in vivo and in vitro studies show that OCT reduces the severity of SAP concentration-dependently.

3.3. OCT decreases the expression of pyroptosis markers in SAP mice

To assess whether OCT mitigates pyroptosis in SAP mice, we conducted a thorough evaluation of the expression of key pyroptosis markers in the pancreas using Quantitative Real-time PCR. As illustrated in Fig. 3a, the elevated levels of ASC, HMGB1, Caspase-1 and GSDMD were notably reduced in a dose-dependent manner with OCT treatment in SAP models. Subsequently, we employed immunofluorescence techniques to investigate further alterations in the protein levels of pyroptosis-related molecules in the pancreas (Fig. 3b–d). These methods revealed substantial changes in the expression patterns of these proteins, confirming the findings obtained through PCR analysis. Moreover, TUNEL staining showed less pancreatic apoptosis in OCT mice than in WT mice during AP (Fig. 3e). Complementing these in vivo findings, our in vitro experiments demonstrated a remarkable decrement in the expression of pyroptosis markers following treatment with OCT concentrations ranging from 0.1 nM to 100 nM (Fig. S2g). Transmission electron microscopy analysis revealed that the cell membrane pores of pancreatic acinar cells in the SAP group exhibited formation and subsequent loss of integrity, accompanied by nuclear consolidation. Conversely, the pancreatic acinar cells in the OCT100 group demonstrated a tendency towards morphological normalization, with both the cell membrane and nuclear membrane remaining intact (Fig. 3f). These results collectively indicate that OCT can suppress pyroptosis in SAP mice.

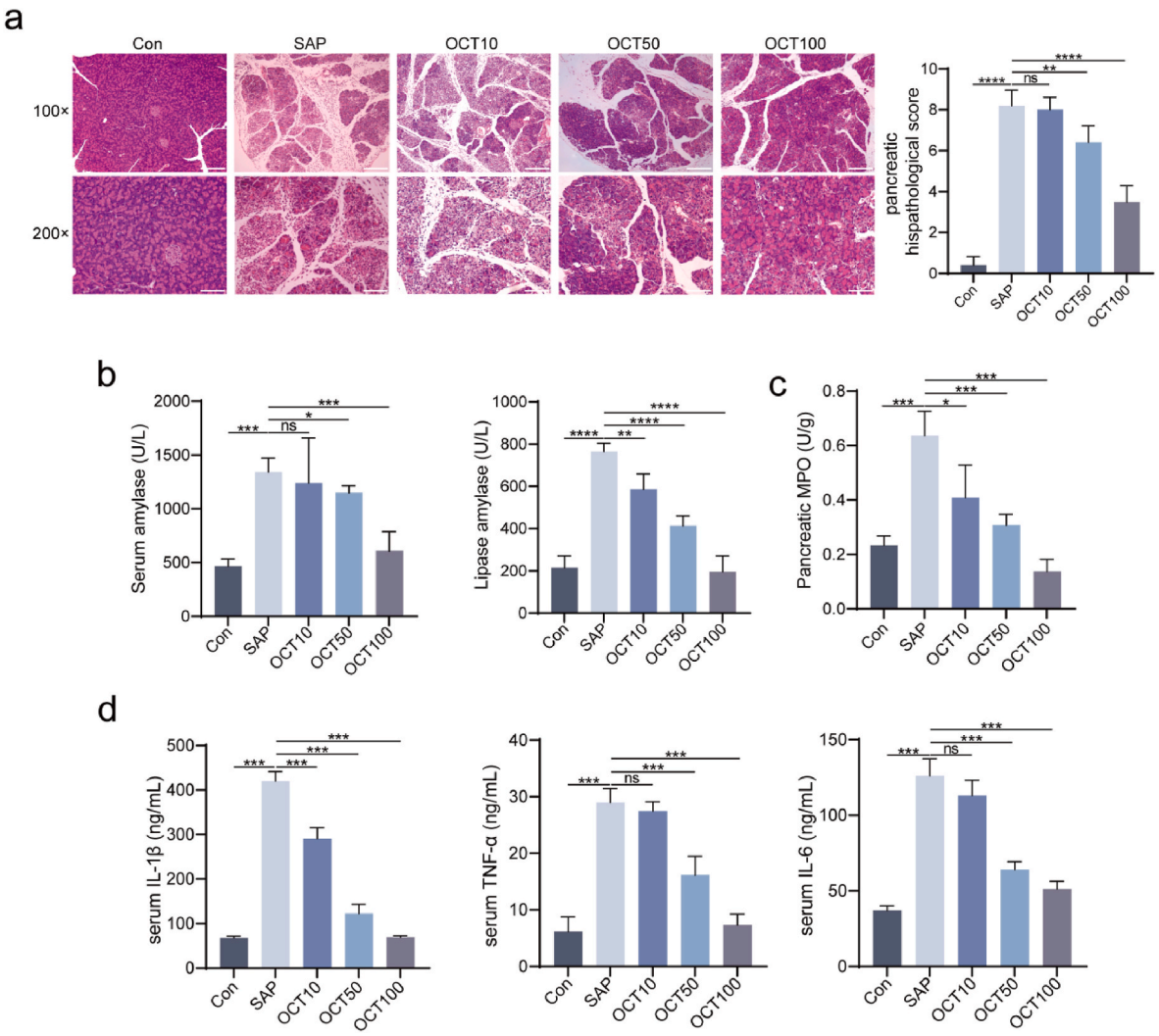

Fig. 2. OCT treatment reduced the severity of SAP. (a) Histopathological changes of pancreas samples observed by HE staining. Original magnification, 100 × (the upper figures) or 200 × (the lower figures) (n = 5 mice per group). **(b)** The level of serum amylase and lipase. **(c)** The pancreatic level of MPO. **(d)** Serum levels of IL-1β, TNF-α and IL-6. The symbol * means P < 0.05, **means P < 0.01, ***means P < 0.001 and ns means P > 0.05.

3.4. OCT effectively alleviates intestinal barrier injury and bacterial translocation during SAP

Compared to the SAP group, the pathological damages in the ileum, such as mucosal injury, inflammation and bleeding, were attenuated in the three OCT groups (Fig. 4a). Analysis of molecules associated with pyroptosis (Caspase-1, GSDMD, NF-kB and TLR4) and inflammatory factors (IL-1β, TNF-α, IL-6 and HMGB1) revealed a marked reduction in their expression in the ileum upon OCT administration (Figs. S3a–h). The results of FISH analysis revealed a notable increase in bacterial translocation in the intestinal mucosa and pancreas of the mice with SAP compared to the control mice. However, treatment with OCT led to a decrease in bacterial translocation in both the intestinal mucosa and pancreas, with the OCT100 group exhibiting the most pronounced decrease (Fig. 4b, Fig. S3i). Subsequently, ileum samples from the Con, SAP and OCT100 groups were chosen for further investigation to assess the potential of OCT in mitigating intestinal barrier damage induced by AP. The expression of tight junction proteins (TJPs), including claudin1, occludin and ZO-1, was examined (Fig. 4c–e). The results indicated a substantial enhancement in the expression of intestinal barrier proteins following OCT treatment.

3.5. OCT treatment modulates the gut microbiota composition in SAP

To further explore the impact of OCT administration on gut microbiota in cases of AP, we conducted additional studies utilizing 16S rRNA sequencing alongside targeted metabolomic analysis. Based on the above results, an OCT concentration of 100 μg/kg was chosen. The mice were then divided into four groups: control (Con), severe acute pancreatitis (SAP), octreotide (OCT) and SAP with octreotide treatment (SAP + OCT). SAP was induced using L-arginine, the OCT group received intraperitoneal injections of 100 μg/kg OCT, and the modeling approach for the SAP + OCT group mirrored that of the previously described OCT100 group.

The Shannon curves indicated that a substantial diversity had been captured in our samples (Fig. S4a). Alpha diversity showed no significant differences among the four groups, except for the Simpson index (Figs. S4b–e). Results from Principal Coordinate Analysis (PCoA) and Principal Component Analysis (PCA) indicated a notable distinction in gut microbiota composition between the OCT group and the other three groups, with the SAP + OCT group positioned closer to the Con group than the SAP group (Fig. 5a, S4f). The Beta diversity difference analysis examines variations between samples, revealing statistically significant differences in gut microbiota among the four groups of mice (Fig. 5b). Hierarchical cluster analysis at the operational taxonomic unit (OTU)

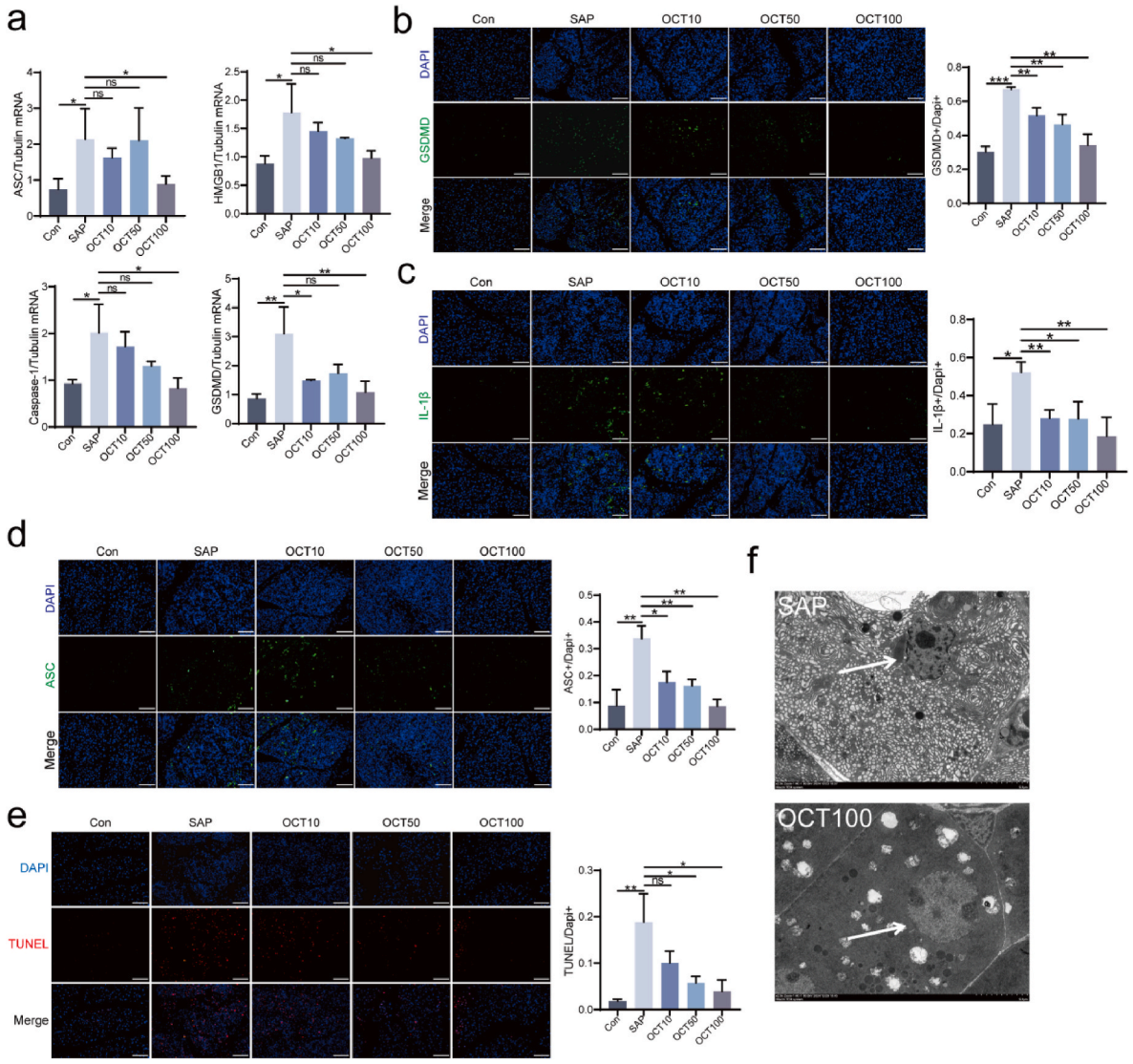

Fig. 3. OCT relieved pyroptosis in SAP mice. (a) The mRNA expression levels of ASC, HMGB1, Caspase-1 and GSDMD in the pancreas. **(b–d)** Immunofluorescence staining and quantification of GSDMD (b) IL-1β (c) ASC (d) in the pancreas (200 × magnification) (n = 5 mice per group). **(e)** TUNEL staining of the pancreas (200 × magnification). **(f)** Ultrastructural comparison by electron microscopy. The symbol * means $P < 0.05$, **means $P < 0.01$, ***means $P < 0.001$ and ns means $P > 0.05$.

level separated the bacteria into distinct branches (Fig. S4g).

Then, we examined alterations in the gut microbiota composition at various taxonomic ranks. Our analysis revealed that the OCT group exhibited reduced levels of *Firmicutes* and elevated levels of *Bacteroides*, *Actinobacteriota* and *Desulfobacterota* at the phylum level. In the SAP + OCT group, the abundance of *Verrucomicrobia* was increased, while the abundance of *Campylobacterota* was decreased compared to the SAP group (Fig. S4h). At the genus level, in comparison to the control group, the SAP group demonstrated a reduction in the abundance of *Oscillibacter*, *Blautia* and *Bacteroides*, while these bacterial populations increased in the SAP group supplemented with OCT (SAP + OCT). Conversely, the abundance of *Desulfovibrio* increased in the SAP group but decreased in the SAP + OCT group. The OCT group exhibited a distinct microbial composition characterized by significantly higher levels of *Odoribacter*, *Desulfovibrio* and *Alistipes* compared to the other groups (Fig. 5c). The analysis of community heatmaps at the genus level confirmed these results and demonstrated that the administration of OCT could effectively reverse the disruptions in bacterial genera caused by SAP, such as *Akkermansia*, Helicobacter, *Alloprevotella* and others (Fig. 5d). These results provide a comprehensive understanding of the influence of OCT administration on the intestinal microbiota during SAP.

Our study revealed that the administration of OCT induces changes in the intestinal microbiota of mice with SAP. Further investigation is needed to determine the correlation between these alterations and the severity of the disease. Circos plots in Fig. S4i are utilized to visually depict the relationship between species and samples, offering a clearer understanding of the distribution of species within the groups. The Gut Microbiome Health Index (GMHI) reliably evaluates health through taxonomic species-level analysis of the gut microbiome, comparing the abundance of favorable and unfavorable microbial species. In contrast, the Microbiome Dysbiosis Index (MDI) measures disruptions in the intestinal microbiota, with a higher MDI indicating greater microbiota disturbance. Examination of two indices indicated that the SAP group exhibited a statistically significant decrease in GMHI and an increase in the MDI group compared to the control group (Fig. 5e and f). GMHI was higher in the OCT group compared to the SAP + OCT group (Fig. 5g); the SAP + OCT had a higher GMHI than the SAP group (Fig. S4j), though the difference was non-significant. The MDI was significantly higher in SAP compared to SAP + OCT (Fig. 5h).

We conducted an analysis comparing two cohorts using the Wilcoxon rank sum test at the genus level to validate the effect of OCT on the SAP

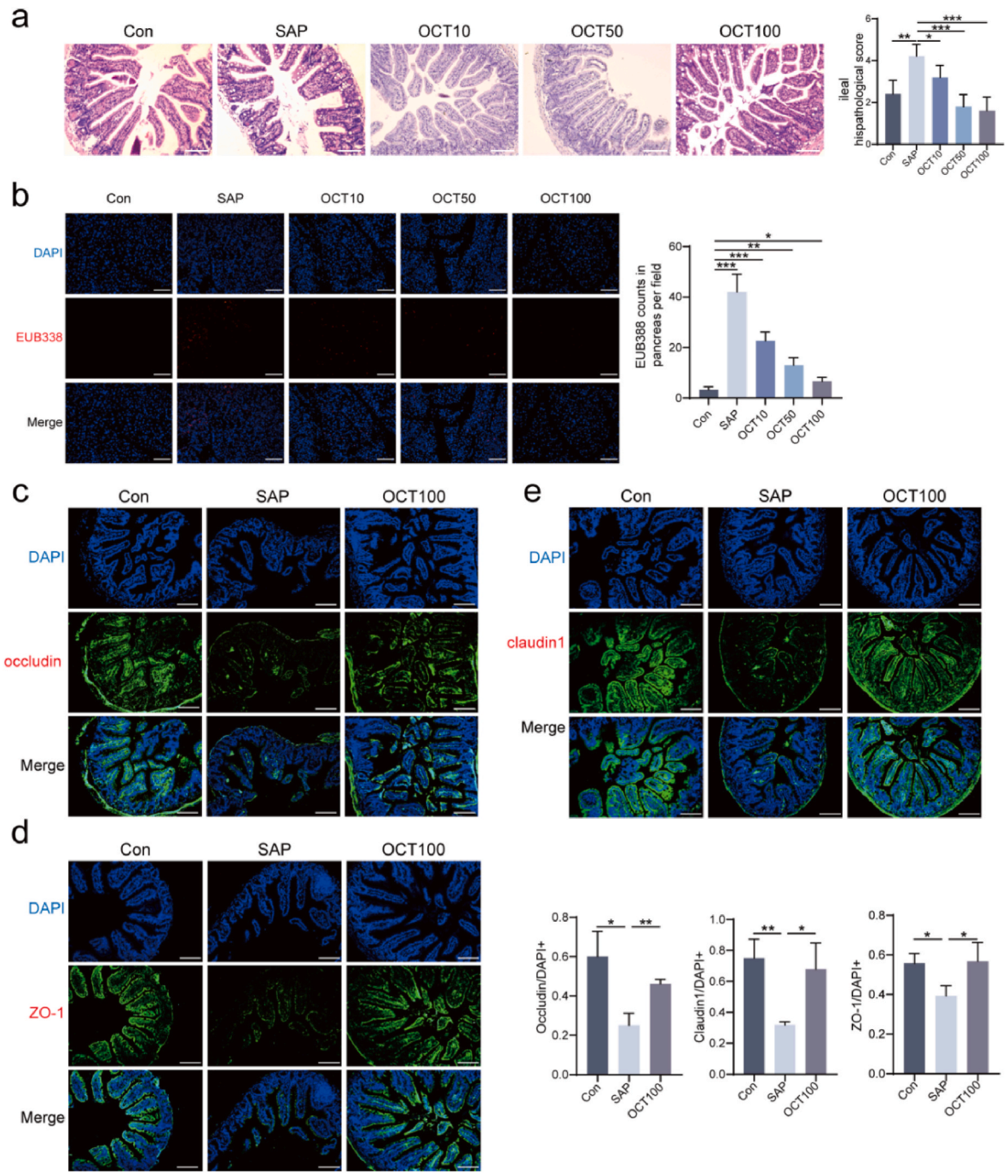

Fig. 4. OCT effectively alleviates intestinal barrier injury and bacterial translocation. (a) Histopathological changes of ileal samples observed by HE staining (200 × magnification) (n = 5 mice per group). **(b)** Positive hybridizing signal of total bacteria detected by the EUB338 probe. The EUB338 counts in the pancreas (200 × magnification) per field were quantified. **(c–e)** Images of ileal occludin, ZO-1 and claudin1 immunofluorescence (200 × magnification) and corresponding cellular quantification (n = 5 mice per group). The symbol * means P < 0.05, **means P < 0.01, ***means P < 0.001 and ns means P > 0.05.

microbiota. The results showed a significant decrease in the prevalence of *Bifidobacterium*, *Lachnospiraceae_FCS020_group* and *unclassified_o_RF39*, and a significant increase in the prevalence of *Marvinbtyantia* in the SAP + OCT group compared to the SAP group (Fig. 5i). Furthermore, a comparative analysis between the control group and the OCT group demonstrated a higher prevalence of the genera *Alistipes*, *Desulfovibrio*, *Odoribacter* and *Enterorhabdus* in the OCT group relative to the control group (Fig. 5j). The Spearman's correlation analysis showed that the inter-genus interactions are complicated (Fig. S5a). According to LEFSe analysis, the Con group was enriched with Clostridia, Firmicutes, Oscillospiraceae, etc.; the SAP group was dominated by Muribaculaceae, Prevotellaceae and Alloprevotella; the SAP + OCT group was enriched with Lachnospiraceae, Akkermansiaceae, Verrucomicrobiota, etc.; the abundance of 27 genera in the OCT group was significantly higher compared with the other three groups (LDA >4, p < 0.05) (Fig. S5b).

3.6. OCT affects metabolic pathways and short-chain fatty acids levels

We conducted one-way ANOVA followed by the Tukey-Kramer multiple comparisons test. Our analysis revealed significant variances in metabolic pathways, particularly in the comparisons between the Con and OCT groups, as well as the SAP and OCT groups (Fig. 6a and b). In

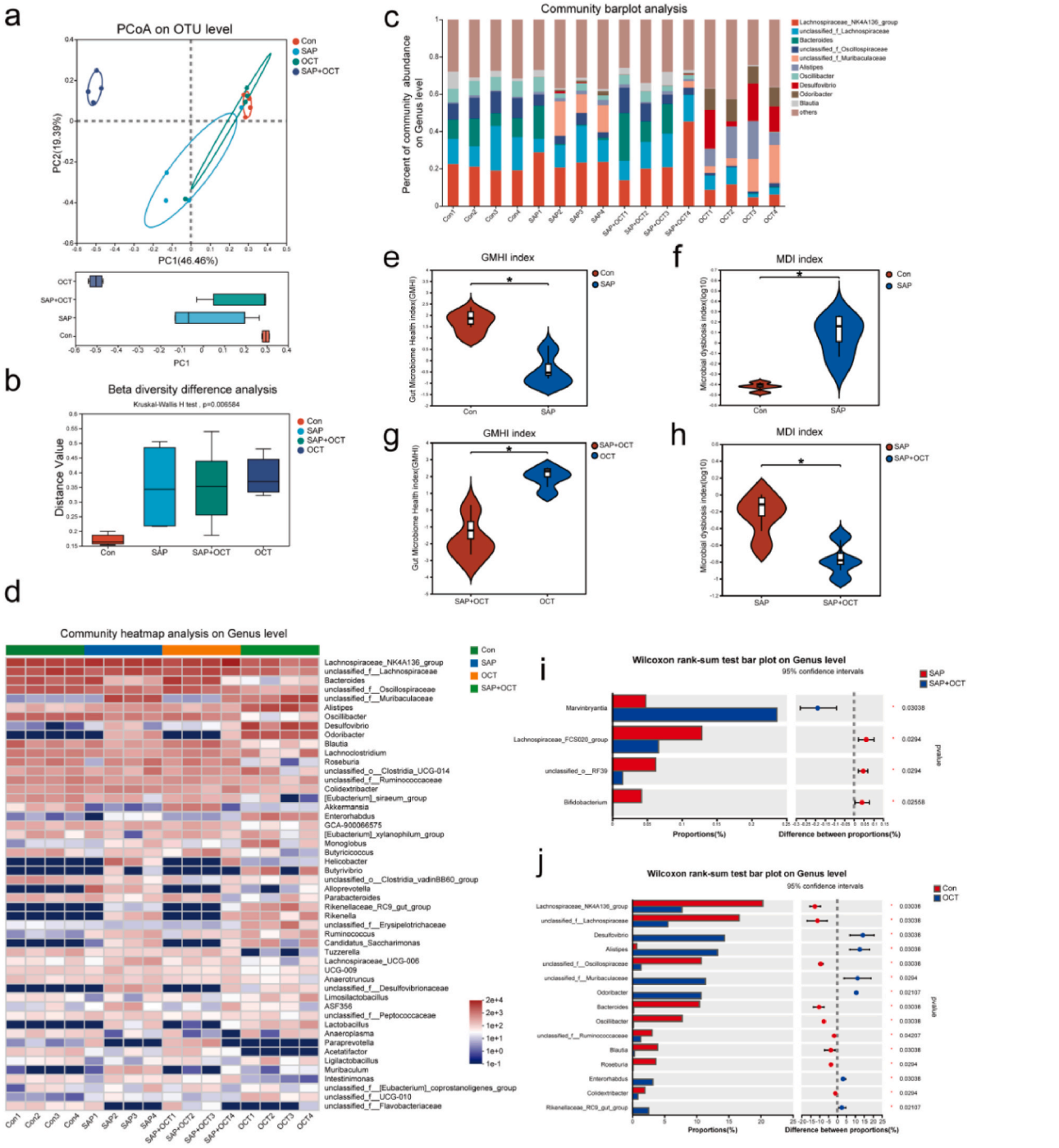

Fig. 5. OCT treatment modulated the gut microbiota composition in SAP. (a) Principal coordinates analysis (PCoA) based on OTU abundance showed the differences in the bacterial microbiota among the four groups. The box plots compare the coordinate positions of the four sets of samples on PC1 and PC2. **(b)** Beta diversity difference analysis. **(c)** The taxonomic composition distribution among the four groups of feces at the genus level. **(d)** Community heatmap analysis on Genus level. **(e)** GMHI between the Con group and the SAP group. **(f)** MDI between the Con group and the SAP group. **(g)** GMHI between the SAP + OCT group and the OCT group. **(h)** MDI between the SAP group and the SAP + OCT group. **(i)** Differences in gut microbiota composition between AP and AP + OCT groups at the genus level. **(j)** Differences in gut microbiota composition between con and OCT groups at the genus level. The symbol * means $P < 0.05$, **means $P < 0.01$, ***means $P < 0.001$ and ns means $P > 0.05$.

this study, we investigated the impact of OCT administration on short-chain fatty acids (SCFAs) levels, as illustrated in Fig. 6c–e. Our findings indicated that, compared to the Con group, OCT administration enhanced the levels of SCFAs, including propanoic acid, acetic acid and butyric acid. These results imply that OCT treatment can modify the composition and metabolic activities of the intestinal microbiota, stimulating the generation of SCFAs and supporting the integrity of the intestinal barrier.

3.7. Validation of the effect of OCT on intestinal microbiota in the caerulein + LPS-induced SAP model

To validate that OCT can improve SAP by modulating gut microbiota, we conducted experiments using caerulein + LPS-induced SAP

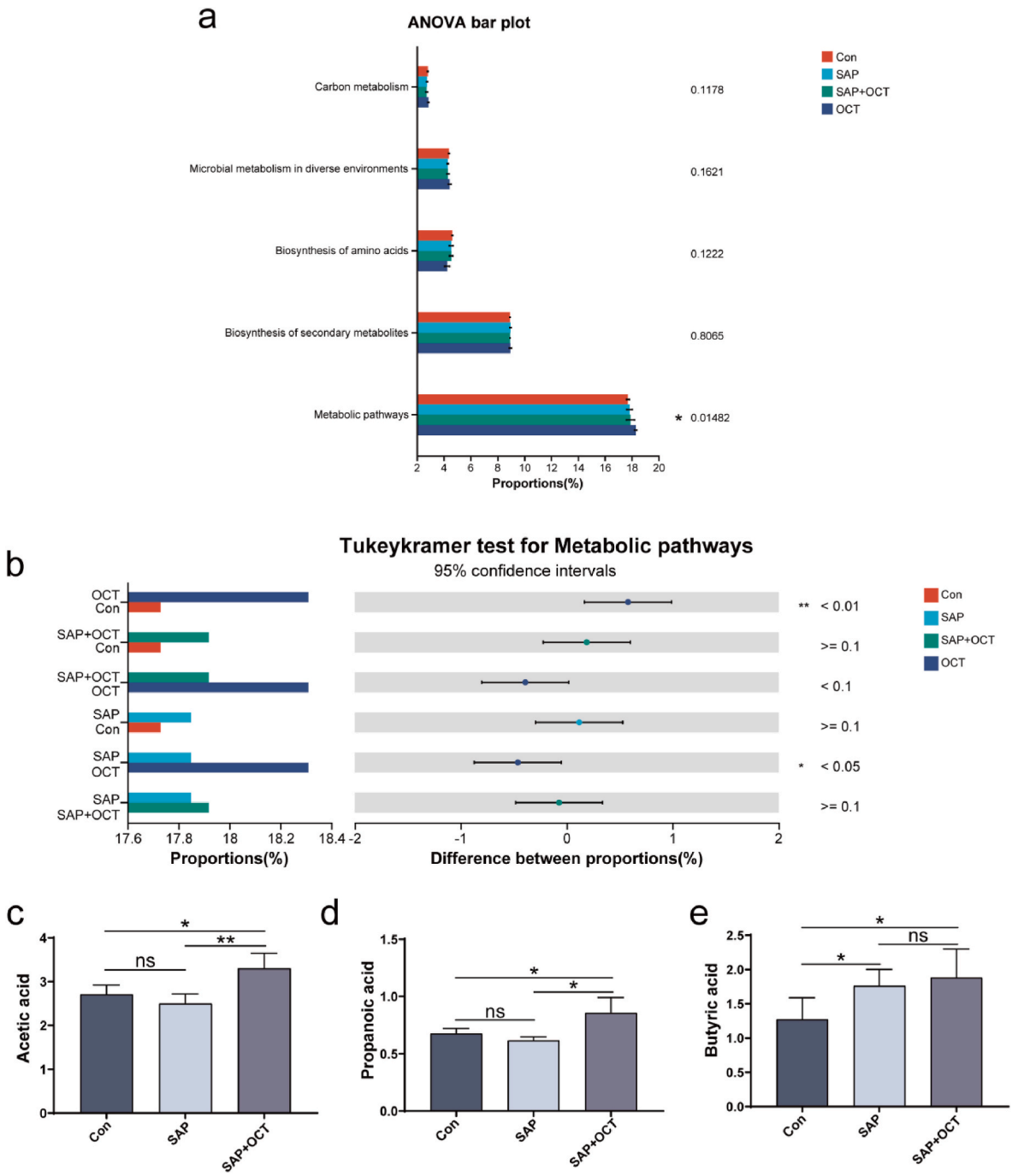

Fig. 6. OCT **affects metabolic pathways. (a)** Four groups of one-way ANOVA bar charts. **(b)** Graph of post-hoc test results. **(c–e)** The fecal levels of SCFAs (propanoic acid, acetic acid and butyric acid) in the three groups of mice. The symbol * means $P < 0.05$, **means $P < 0.01$, ***means $P < 0.001$ and ns means $P > 0.05$.

mice. The mice were divided into three groups: Con, SAP-C and OCT + SAP-C. The modeling modalities for the SAP-C and OCT + SAP-C groups are detailed in the experimental design. Our findings demonstrate that OCT mitigates pancreatic pathologic injury and the level of serum amylase (Fig. 7a and b). Consistent with the findings observed in L-arginine-induced SAP mice, OCT suppressed the expression of pyroptosis markers and inflammatory factors in pancreatic tissues, indicating that OCT effectively ameliorates caerulein + LPS-induced SAP (Figs. S6a and b).

To further elucidate the role of gut microbiota in this process, fecal samples were collected from mice in the Con, SAP-C, OCT and OCT + SAP-C groups, processed into a bacterial suspension, and subsequently administered to antibiotic-treated (ABX) mice via gavage for one week. These ABX mice were then designated as FMT-Con, FMT-SAP-C, FMT-OCT and FMT-OCT + SAP-C groups, respectively. Our findings revealed that pancreatic pathologic damage was most severe in the FMT-SAP-C group, whereas it was reduced in the FMT-OCT + SAP-C group (Fig. 7c). However, there were no statistically significant differences in serum amylase levels between the three experimental groups and the control group (Fig. 7d). In the pancreas of mice in the FMT-SAP-C group, there was an elevation in inflammatory factors and markers of pyroptosis, while the other three groups showed a noticeable decrease in these markers (Figs. S6c and d). Examination of the expression of intestinal barrier proteins revealed that disruptions in the intestinal microecology,

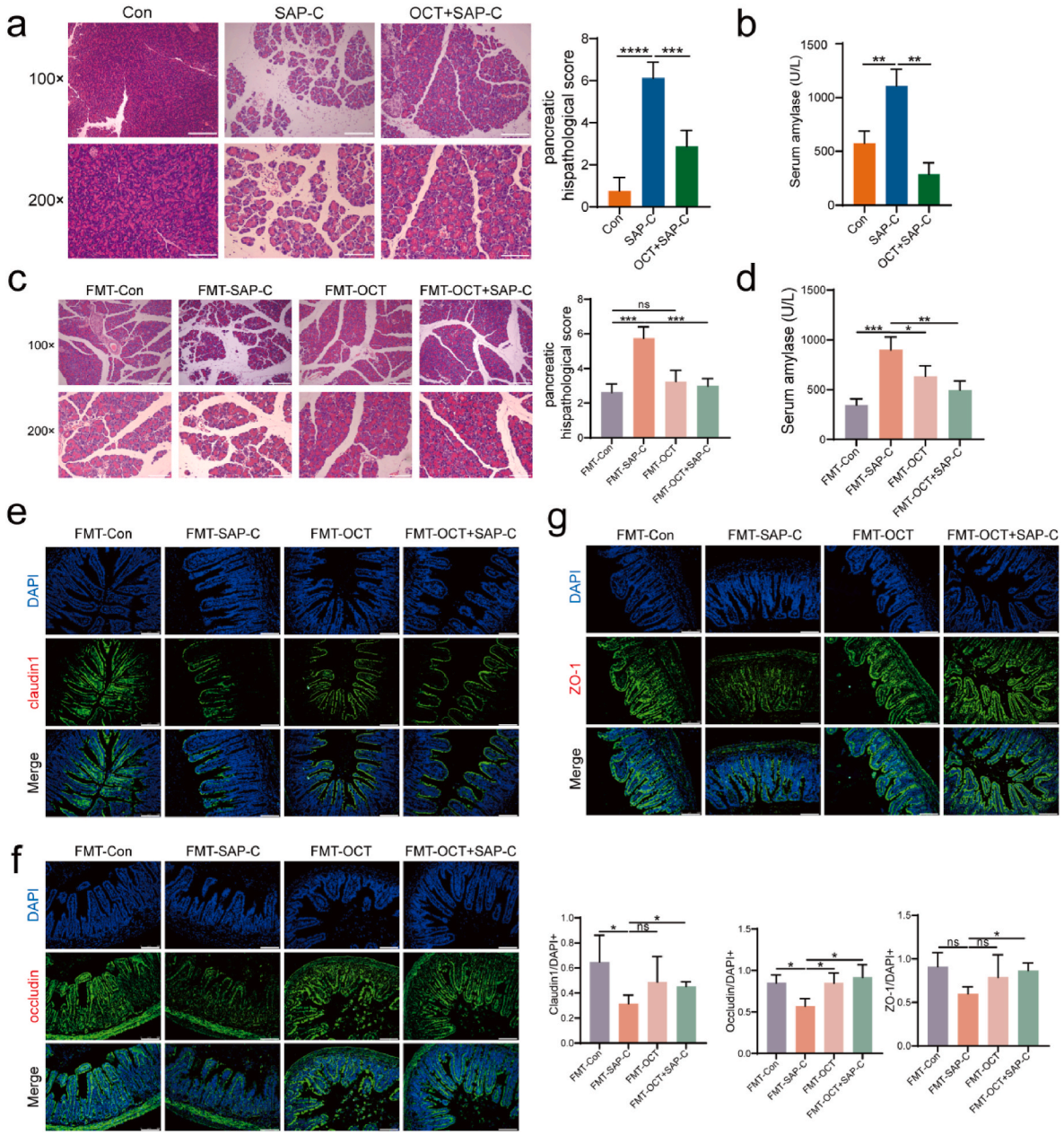

Fig. 7. OCT relieved the severity of caerulein + LPS-induced SAP mice. (a, c) Histopathological changes of pancreas samples observed by HE staining. Original magnification, 100 × (the upper figures) or 200 × (the lower figures) (n = 4 mice per group). **(a)** Histopathological changes of pancreas samples observed by HE staining. Original magnification, 100 × (the upper figures) or 200 × (the lower figures) (n = 4 mice per group). **(b, d)** The level of serum amylase. **(e–g)** Images of ileal occludin, claudin1 and ZO-1 immunofluorescence (200 × magnification) and corresponding cellular quantification (n = 4 mice per group). Symbol * means P < 0.05, **means P < 0.01, ***means P < 0.001, ns means P > 0.05.

induced by caerulein + LPS-induced SAP, also led to impairments in the intestinal barrier. Additionally, OCT administration appeared to partially restore the intestinal barrier (Fig. 7e–g). These findings provide further evidence of OCT in treating SAP through modulation of gut microbiota.

4. Discussion

OCT is widely used in clinical pancreatitis patients, but its specific mechanism of action remains unclear. This study involved a thorough examination of the protective mechanisms of OCT in mice with two different experimentally induced models of SAP. The results suggest that OCT administration not only effectively modulates signaling pathways in the pancreas associated with pyroptosis, but also mitigates SAP through the regulation of gut microbiota and its metabolism. Furthermore, OCT's potential to ameliorate pancreatic injury in SAP was highlighted by its ability to reduce disruption of the intestinal barrier and translocation of bacteria. The combination of OCT's anti-pyroptotic properties and its ability to maintain intestinal homeostasis plays a crucial role in alleviating the severity of SAP.

Pyroptosis, a form of inflammasome-induced programmed cell death, involves the sequential activation of the inflammasome, pro-caspase-1 and precursor forms of IL-1β and IL-18 (Vasudevan et al., 2023). Upon activation, caspase-1 cleaves GSDMD protein molecules, leading to the formation of membrane pores that promote the uncontrolled release of inflammatory mediators and cellular infiltration, ultimately resulting in pyroptosis (Liu et al., 2021b). In our prior study, heightened levels of pyroptosis-associated molecules were observed in

the pancreatic tissue of mice induced with SAP through the administration of L-arginine or caerulein + LPS. Subsequent research has provided additional evidence for supporting the pivotal involvement of pyroptosis in AP (Ferrero-Andres et al., 2020; Kang et al., 2014; Wu et al., 2020). In this study, we observed the effects of inhibiting in vivo pyroptosis on SAP in mice using disulfiram, a drug proven to safely prevent GSDMD-mediated pyroptosis by modulating multiple stages of the process. The findings demonstrated that disulfiram alleviated pathological damage and reduced the inflammatory response in SAP. Furthermore, existing research has shown that a range of inflammatory diseases, including AP, can be attenuated by inhibiting pyroptosis (Coll et al., 2022; Hou et al., 2019).

OCT is a commonly utilized pharmaceutical agent in clinical practice for the management of AP. This study investigates the underlying mechanism of action responsible for the therapeutic efficacy of OCT in AP by employing a combination of in vivo and in vitro methodologies, as well as genetic and pharmacological interventions targeting key pyroptosis pathways. Research has shown that OCT mitigates hepatic ischemia/reperfusion (HIR) injury through its targeting of NLRP3 inflammasome-induced pyroptosis (El-Sisi et al., 2021). Given the relationship between acute pancreatitis and pyroptosis, we conducted additional investigations to ascertain whether OCT, a frequently utilized pharmaceutical agent, ameliorates acute pancreatitis by suppressing the pyroptosis pathway. In the in vivo component of the study, we evaluated the response of arginine-induced SAP mice to varying concentrations of OCT, specifically OCT10, OCT50 and OCT100. OCT was administered at concentrations of 10 μg/kg, 50 μg/kg and 100 μg/kg, respectively. Our results demonstrate that OCT exerts a concentration-dependent reduction in SAP severity and concomitantly suppresses pyroptosis expression. Interestingly, in comparison to SAP mice, the remission effect in the OCT10 group was occasionally statistically insignificant. This observation is consistent with the findings of a randomized controlled trial, which showed no significant difference between the control group and the low-concentration OCT group in the prevention and treatment of SAP (Wang et al., 2013b). Similarly, several studies have demonstrated that administering high doses of OCT can effectively prevent post-ERCP pancreatitis (Andriulli, 2007). In vitro experiments also supported these results, showing that OCT reduced pyroptosis and inflammatory response in pancreatic acinar cells in a concentration-dependent manner within a specific range. LDH levels are a predictor of pyroptotic cell death (Luo et al., 2023). To validate the therapeutic efficacy of high-dose OCT in the treatment of SAP, we used SAP mice induced by caerulein + LPS. Consistently, OCT100 effectively attenuated pancreatic injury, reduced the inflammatory response and decreased the expression of pyroptosis in SAP mice. Ulinastatin functions as a trypsin inhibitor and exhibits therapeutic potential in the treatment of pancreatitis, as well as in the inhibition of pyroptosis (Huang et al., 2024; Pan et al., 2017). The experimental findings of this study indicated that Ulinastatin mitigated pancreatic injury and reduced cellular pyroptosis; however, the effects of OCT100 were notably more pronounced. Research has demonstrated that the clinical efficacy of Ulinastatin is constrained by the presence and limited specificity of the blood-pancreas barrier (BPB) (Chen et al., 2023). Furthermore, evidence suggests that while somatostatin is effective in the management of acute pancreatitis, Ulinastatin has only shown modest improvements in outcomes (Wang et al., 2013a, 2016).

In the pathogenesis of AP, there exists a complex interconnection and mutual influence between pancreatic and intestinal injuries. The disruption of the biological barrier established by the gastrointestinal microecology during AP leads to a shift towards microbiota dysbiosis. This dysbiosis allows for the migration of disrupted microbial communities through the compromised intestinal barrier, thereby exacerbating the severity of AP (Liu et al., 2024; Qi-Xiang et al., 2022). Furthermore, studies have shown that the interaction between gut microbiota and NLRP3 inflammasome significantly impacts the severity of AP (Li et al., 2020; Yang et al., 2024). The findings of our experiment provide additional evidence supporting the notion that the intestinal barrier is compromised and the composition of the intestinal microecology is altered after the induction of SAP in mice. Nevertheless, the administration of OCT effectively mitigates intestinal damage, restores barrier function, and may prevent the translocation of microbiota to the pancreas. Through the analysis of microbiota composition, we discovered that the administration of OCT effectively reversed multiple disruptions in the intestinal microbiota induced by SAP. Specifically, the SAP + OCT group displayed a higher abundance of *Oscillibacter*, *Blautia*, *Bacteroides*, *Paraprevotella* and *Akkermansia* compared to the SAP group, while the abundance of *Desulfovibrio*, Helicobacter, *Alloprevotella* and other bacteria decreased. In contrast, the OCT group had a different microbial composition, with considerably higher levels of *Odoribacter*, *Desulfovibrio*, *Alistipes* and u*nclassified_f_Muribaculaceae* than the other groups. Research has shown a correlation between an elevation in the prevalence of *Oscillibacter* and *Alistipes* and a reduction in triglyceride levels (Liu et al., 2022b). *Oscillibacter* has been identified as being linked to SAP in a study, suggesting its potential as a novel predictive marker for SAP (Wang et al., 2023). *Blautia*, *Akkermansia* and *Odoribacter* are identified as probiotics essential for maintaining intestinal equilibrium, enhancing the immune system, metabolism and intestinal barrier function of the host (Cani et al., 2022; Liu et al., 2021a; Zhou et al., 2022). They have been recognized for their significant role in the pathogenesis of acute pancreatitis (Fu et al., 2022; Wang et al., 2024). Conversely, *Desulfovibrio* and *Helicobacter* are recognized as pathogenic bacteria capable of inducing a range of gastrointestinal ailments (Sayavedra et al., 2021; Sun et al., 2023), while *Alloprevotella* is considered a potential oral biomarker in intestinal metaphase of gastric patients (Liu et al., 2023). *Helicobacter* is believed to be associated with various pancreatic diseases, such as autoimmune pancreatitis and pancreatic cancer (Hurtado-Monzon et al., 2024; Kunovsky et al., 2021), while studies have reported the presence of *Alloprevotella* in reductions of hypertriglyceridemia-associated acute necrotizing pancreatitis (ANP) (Huang et al., 2017).

The present study offers substantial evidence supporting the hypothesis that the administration of OCT in SAP fosters a favorable microenvironment that augments beneficial bacteria while containing pathogenic strains. This finding aligns with the outcomes of the GMHI and MDI. However, it was observed that the microbiota composition in the OCT group (where only OCT was administered) exhibited greater complexity, featuring a substantial surge in both beneficial and harmful bacteria. Further scrutiny is needed to elucidate the mechanisms behind this observation. *Blautia*, *Akkermansia* and *Muribaculaceae* are acknowledged as significant producers of short-chain fatty acids (SCFAs), which are well-known for their therapeutic effects in a variety of diseases, including the mitigation of AP (van den Berg et al., 2021; Xia et al., 2023). In light of this, a targeted metabolomic analysis was performed on fecal samples obtained from three distinct mouse cohorts. The results revealed a higher level of SCFAs production in the SAP + OCT group compared to the SAP group. A one-way ANOVA analysis revealed statistically significant differences in metabolic pathways, suggesting the presence of alternative metabolic routes deserving further investigation. The results outlined in this section demonstrate that OCT therapy for SAP successfully rectifies disruptions in intestinal microecology and alters related metabolic pathways. Our study further confirmed the influence of OCT on intestinal microecology in mice with CAE + LPS-induced SAP. By manipulating the intestinal microbiota composition in ABX mice using FMT, we found that the FMT-SAP-C group exhibited the most severe intestinal barrier damage and pancreatic inflammation. These results offer additional support for the negative impact of SAP on intestinal microecology and highlight the regulatory function of OCT.

In this study, we discovered that OCT exhibits a concentration-dependent attenuation of the severity of SAP and reduces the expression of pancreatic pyroptosis markers. Furthermore, OCT has been shown to mitigate SAP-induced damage to the intestinal barrier and restore disruptions in intestinal microecology. By elucidating these

mechanisms, we aim to better understand octreotide's therapeutic potential and identify innovative approaches for SAP treatment.

CRediT authorship contribution statement

Mengqi Zhao: Writing – review & editing, Writing – original draft, Validation, Software, Methodology, Formal analysis, Data curation. **Mengyan Cui:** Validation, Software, Data curation. **Miaoyan Fan:** Formal analysis, Data curation. **Chunlan Huang:** Validation, Methodology, Formal analysis. **Jingjing Wang:** Writing – review & editing, Conceptualization. **Yue Zeng:** Validation, Resources, Formal analysis, Data curation. **Xingpeng Wang:** Supervision, Project administration, Funding acquisition, Conceptualization. **Yingying Lu:** Writing – review & editing, Funding acquisition, Conceptualization.

Funding

This work was supported by the Shanghai Natural Science Foundation Project, grant number 22ZR1453500, the Jiading District Health Commission Scientific Project (Grant No. 2023-KY-01) and the Jiading District Health Commission Scientific Project (Grant No. 2022-KY-01).

Declaration of competing interest

We confirm that the manuscript has been read and approved by all named authors and that there are no other persons who satisfied the criteria for authorship but are not listed. We further confirm that the order of authors listed in the manuscript has been approved by all of us. We have given due consideration to the protection of intellectual property associated with this work and that there are no impediments to publication. We confirm that there are no known conflicts of interest associated with this publication and there has been no significant financial support for this work that could have influenced its outcome. The authors declare no competing financial interests.

Acknowledgements

We are grateful to the contributors to the public databases used in this study. We would like to thank the Shanghai Key Laboratory of Pancreatic Diseases, Institute of Translational Medicine, Shanghai General Hospital, Shanghai Jiao Tong University School of Medicine.

Appendix A. Supplementary data

Supplementary data to this article can be found online at https://doi.org/10.1016/j.ejphar.2025.177314.

Data availability

Data will be made available on request.

References

Andriulli, A., 2007. High dose of octreotide as a prophylaxis of post-ERCP pancreatitis. Gastrointest. Endosc. 66. https://doi.org/10.1016/j.gie.2007.02.009, 421; author reply 421-2.

Banks, P.A., Bollen, T.L., Dervenis, C., Gooszen, H.G., Johnson, C.D., Sarr, M.G., Tsiotos, G.G., Vege, S.S., Acute Pancreatitis Classification Working, G., 2013. Classification of acute pancreatitis–2012: revision of the Atlanta classification and definitions by international consensus. Gut 62, 102–111. https://doi.org/10.1136/gutjnl-2012-302779.

Barreto, S.G., Habtezion, A., Gukovskaya, A., Lugea, A., Jeon, C., Yadav, D., Hegyi, P., Venglovecz, V., Sutton, R., Pandol, S.J., 2021. Critical thresholds: key to unlocking the door to the prevention and specific treatments for acute pancreatitis. Gut 70, 194–203. https://doi.org/10.1136/gutjnl-2020-322163.

Borzsei, R., Borbely, E., Kantas, B., Hudhud, L., Horvath, A., Szoke, E., Hetenyi, C., Helyes, Z., Pinter, E., 2023. The heptapeptide somatostatin analogue TT-232 exerts analgesic and anti-inflammatory actions via SST(4) receptor activation: in silico, in vitro and in vivo evidence in mice. Biochem. Pharmacol. 209, 115419. https://doi.org/10.1016/j.bcp.2023.115419.

Cani, P.D., Depommier, C., Derrien, M., Everard, A., de Vos, W.M., 2022. Akkermansia muciniphila: paradigm for next-generation beneficial microorganisms. Nat. Rev. Gastroenterol. Hepatol. 19, 625–637. https://doi.org/10.1038/s41575-022-00631-9.

Chen, Y., Tao, H., Chen, R., Pan, Y., Wang, J., Gao, R., Chen, J., Yang, J., 2023. Biomimetic nanoparticles loaded with ulinastatin for the targeted treatment of acute pancreatitis. Mol. Pharm. 20, 4108–4119. https://doi.org/10.1021/acs.molpharmaceut.3c00238.

Coll, R.C., Schroder, K., Pelegrin, P., 2022. NLRP3 and pyroptosis blockers for treating inflammatory diseases. Trends Pharmacol. Sci. 43, 653–668. https://doi.org/10.1016/j.tips.2022.04.003.

Dawra, R., Sharif, R., Phillips, P., Dudeja, V., Dhaulakhandi, D., Saluja, A.K., 2007. Development of a new mouse model of acute pancreatitis induced by administration of L-arginine. Am. J. Physiol. Gastrointest. Liver Physiol. 292, G1009–G1018. https://doi.org/10.1152/ajpgi.00167.2006.

El-Sisi, A.E.E., Sokar, S.S., Shebl, A.M., Mohamed, D.Z., Abu-Risha, S.E., 2021. Octreotide and melatonin alleviate inflammasome-induced pyroptosis through inhibition of TLR4-NF-kappaB-NLRP3 pathway in hepatic ischemia/reperfusion injury. Toxicol. Appl. Pharmacol. 410, 115340. https://doi.org/10.1016/j.taap.2020.115340.

Fan, R., Sui, J., Dong, X., Jing, B., Gao, Z., 2021. Wedelolactone alleviates acute pancreatitis and associated lung injury via GPX4 mediated suppression of pyroptosis and ferroptosis. Free Radic. Biol. Med. 173, 29–40. https://doi.org/10.1016/j.freeradbiomed.2021.07.009.

Ferrero-Andres, A., Panisello-Rosello, A., Rosello-Catafau, J., Folch-Puy, E., 2020. NLRP3 inflammasome-mediated inflammation in acute pancreatitis. Int. J. Mol. Sci. 21. https://doi.org/10.3390/ijms21155386.

Fu, Y., Mei, Q., Yin, N., Huang, Z., Li, B., Luo, S., Xu, B., Fan, J., Huang, C., Zeng, Y., 2022. Paneth cells protect against acute pancreatitis via modulating gut microbiota dysbiosis. mSystems 7, e0150721. https://doi.org/10.1128/msystems.01507-21.

Gao, L., Dong, X., Gong, W., Huang, W., Xue, J., Zhu, Q., Ma, N., Chen, W., Fu, X., Gao, X., Lin, Z., Ding, Y., Shi, J., Tong, Z., Liu, T., Mukherjee, R., Sutton, R., Lu, G., Li, W., 2021. Acinar cell NLRP3 inflammasome and gasdermin D (GSDMD) activation mediates pyroptosis and systemic inflammation in acute pancreatitis. Br. J. Pharmacol. 178, 3533–3552. https://doi.org/10.1111/bph.15499.

Hou, C., Zhu, X., Shi, C., Peng, Y., Huang, D., Li, Q., Miao, Y., 2019. Iguratimod (T-614) attenuates severe acute pancreatitis by inhibiting the NLRP3 inflammasome and NF-kappaB pathway. Biomed. Pharmacother. 119, 109455. https://doi.org/10.1016/j.biopha.2019.109455.

Huang, C., Chen, J., Wang, J., Zhou, H., Lu, Y., Lou, L., Zheng, J., Tian, L., Wang, X., Cao, Z., Zeng, Y., 2017. Dysbiosis of intestinal microbiota and decreased antimicrobial peptide level in paneth cells during hypertriglyceridemia-related acute necrotizing pancreatitis in rats. Front. Microbiol. 8, 776. https://doi.org/10.3389/fmicb.2017.00776.

Huang, W., Zhang, H., Wang, L., Zhang, F., Ma, M., Chen, D., Wan, X., Zhang, Y., Cao, C., 2024. Ulinastatin attenuates renal ischemia-reperfusion injury by inhibiting NLRP3 inflammasome-triggered pyroptosis. Int. Immunopharmacol. 143, 113306. https://doi.org/10.1016/j.intimp.2024.113306.

Hurtado-Monzon, E.G., Valencia-Mayoral, P., Silva-Olivares, A., Banuelos, C., Velazquez-Guadarrama, N., Betanzos, A., 2024. The Helicobacter pylori infection alters the intercellular junctions on the pancreas of gerbils (Meriones unguiculatus). World J. Microbiol. Biotechnol. 40, 273. https://doi.org/10.1007/s11274-024-04081-0.

Kang, R., Lotze, M.T., Zeh, H.J., Billiar, T.R., Tang, D., 2014. Cell death and DAMPs in acute pancreatitis. Mol. Med. 20, 466–477. https://doi.org/10.2119/molmed.2014.00117.

Kunovsky, L., Dite, P., Jabandziev, P., Dolina, J., Vaculova, J., Blaho, M., Bojkova, M., Dvorackova, J., Uvirova, M., Kala, Z., Trna, J., 2021. Helicobacter pylori infection and other bacteria in pancreatic cancer and autoimmune pancreatitis. World J. Gastrointest. Oncol. 13, 835–844. https://doi.org/10.4251/wjgo.v13.i8.835.

La Salvia, A., Modica, R., Rossi, R.E., Spada, F., Rinzivillo, M., Panzuto, F., Faggiano, A., Cinieri, S., Fazio, N., 2023. Targeting neuroendocrine tumors with octreotide and lanreotide: key points for clinical practice from NET specialists. Cancer Treat Rev. 117, 102560. https://doi.org/10.1016/j.ctrv.2023.102560.

Lerch, M.M., Gorelick, F.S., 2013. Models of acute and chronic pancreatitis. Gastroenterology 144, 1180–1193. https://doi.org/10.1053/j.gastro.2012.12.043.

Li, X., He, C., Li, N., Ding, L., Chen, H., Wan, J., Yang, X., Xia, L., He, W., Xiong, H., Shu, X., Zhu, Y., Lu, N., 2020. The interplay between the gut microbiota and NLRP3 activation affects the severity of acute pancreatitis in mice. Gut Microbes 11, 1774–1789. https://doi.org/10.1080/19490976.2020.1770042.

Li, Z.S., Pan, X., Zhang, W.J., Gong, B., Zhi, F.C., Guo, X.G., Li, P.M., Fan, Z.N., Sun, W.S., Shen, Y.Z., Ma, S.R., Xie, W.F., Chen, M.H., Li, Y.Q., 2007. Effect of octreotide administration in the prophylaxis of post-ERCP pancreatitis and hyperamylasemia: a multicenter, placebo-controlled, randomized clinical trial. Am. J. Gastroenterol. 102, 46–51. https://doi.org/10.1111/j.1572-0241.2006.00959.x.

Liu, D., Wen, L., Wang, Z., Hai, Y., Yang, D., Zhang, Y., Bai, M., Song, B., Wang, Y., 2022a. The mechanism of lung and intestinal injury in acute pancreatitis: a review. Front. Med. 9, 904078. https://doi.org/10.3389/fmed.2022.904078.

Liu, J., Huang, L., Luo, M., Xia, X., 2019. Bacterial translocation in acute pancreatitis. Crit. Rev. Microbiol. 45, 539–547. https://doi.org/10.1080/1040841X.2019.1621795.

Liu, J., Yan, Q., Li, S., Jiao, J., Hao, Y., Zhang, G., Zhang, Q., Luo, F., Zhang, Y., Lv, Q., Zhang, W., Zhang, A., Song, H., Xin, Y., Ma, Y., Owusu, L., Ma, X., Yin, P., Shang, D., 2024. Integrative metagenomic and metabolomic analyses reveal the potential of gut microbiota to exacerbate acute pancreatitis. NPJ Biofilms Microbiomes 10, 29. https://doi.org/10.1038/s41522-024-00499-4.

Liu, X., Mao, B., Gu, J., Wu, J., Cui, S., Wang, G., Zhao, J., Zhang, H., Chen, W., 2021a. Blautia-a new functional genus with potential probiotic properties? Gut Microbes 13, 1–21. https://doi.org/10.1080/19490976.2021.1875796.

Liu, X., Tong, X., Zou, Y., Lin, X., Zhao, H., Tian, L., Jie, Z., Wang, Q., Zhang, Z., Lu, H., Xiao, L., Qiu, X., Zi, J., Wang, R., Xu, X., Yang, H., Wang, J., Zong, Y., Liu, W., Hou, Y., Zhu, S., Jia, H., Zhang, T., 2022b. Mendelian randomization analyses support causal relationships between blood metabolites and the gut microbiome. Nat. Genet. 54, 52–61. https://doi.org/10.1038/s41588-021-00968-y.

Liu, X., Xia, S., Zhang, Z., Wu, H., Lieberman, J., 2021b. Channelling inflammation: gasdermins in physiology and disease. Nat. Rev. Drug Discov. 20, 384–405. https://doi.org/10.1038/s41573-021-00154-z.

Liu, Y., Wang, H., Jiang, H., Sun, Z., Sun, A., 2023. Alloprevotella can be considered as a potential oral biomarker in intestinal metaphase of gastric patients. Stud. Health Technol. Inf. 308, 155–167. https://doi.org/10.3233/SHTI230836.

Luo, T., Jia, X., Feng, W.D., Wang, J.Y., Xie, F., Kong, L.D., Wang, X.J., Lian, R., Liu, X., Chu, Y.J., Wang, Y., Xu, A.L., 2023. Bergapten inhibits NLRP3 inflammasome activation and pyroptosis via promoting mitophagy. Acta Pharmacol. Sin. 44, 1867–1878. https://doi.org/10.1038/s41401-023-01094-7.

Mohamed, D.Z., El-Sisi, A.E.E., Sokar, S.S., Shebl, A.M., Abu-Risha, S.E., 2021. Targeting autophagy to modulate hepatic ischemia/reperfusion injury: a comparative study between octreotide and melatonin as autophagy modulators through AMPK/PI3K/AKT/mTOR/ULK1 and Keap1/Nrf2 signaling pathways in rats. Eur. J. Pharmacol. 897, 173920. https://doi.org/10.1016/j.ejphar.2021.173920.

Pan, Y., Fang, H., Lu, F., Pan, M., Chen, F., Xiong, P., Yao, Y., Huang, H., 2017. Ulinastatin ameliorates tissue damage of severe acute pancreatitis through modulating regulatory T cells. J. Inflamm. 14, 7. https://doi.org/10.1186/s12950-017-0154-7.

Petrov, M.S., Yadav, D., 2019. Global epidemiology and holistic prevention of pancreatitis. Nat. Rev. Gastroenterol. Hepatol. 16, 175–184. https://doi.org/10.1038/s41575-018-0087-5.

Qi-Xiang, M., Yang, F., Ze-Hua, H., Nuo-Ming, Y., Rui-Long, W., Bin-Qiang, X., Jun-Jie, F., Chun-Lan, H., Yue, Z., 2022. Intestinal TLR4 deletion exacerbates acute pancreatitis through gut microbiota dysbiosis and Paneth cells deficiency. Gut Microbes 14, 2112882. https://doi.org/10.1080/19490976.2022.2112882.

Sayavedra, L., Li, T., Bueno Batista, M., Seah, B.K.B., Booth, C., Zhai, Q., Chen, W., Narbad, A., 2021. Desulfovibrio diazotrophicus sp. nov., a sulfate-reducing bacterium from the human gut capable of nitrogen fixation. Environ. Microbiol. 23, 3164–3181. https://doi.org/10.1111/1462-2920.15538.

Schepers, N.J., Bakker, O.J., Besselink, M.G., Ahmed Ali, U., Bollen, T.L., Gooszen, H.G., van Santvoort, H.C., Bruno, M.J., Dutch Pancreatitis Study, G., 2019. Impact of characteristics of organ failure and infected necrosis on mortality in necrotising pancreatitis. Gut 68, 1044–1051. https://doi.org/10.1136/gutjnl-2017-314657.

Shimizu, T., Shiratori, K., Sawada, T., Kobayashi, M., Hayashi, N., Saotome, H., Keith, J. C., 2000. Recombinant human interleukin-11 decreases severity of acute necrotizing pancreatitis in mice. Pancreas 21, 134–140. https://doi.org/10.1097/00006676-200008000-00005.

Smith, K.M., Mrozek, J.D., Simonton, S.C., Bing, D.R., Meyers, P.A., Connett, J.E., Mammel, M.C., 1997. Prolonged partial liquid ventilation using conventional and high-frequency ventilatory techniques: gas exchange and lung pathology in an animal model of respiratory distress syndrome. Crit. Care Med. 25, 1888–1897. https://doi.org/10.1097/00003246-199711000-00030.

Sun, Q., Yuan, C., Zhou, S., Lu, J., Zeng, M., Cai, X., Song, H., 2023. Helicobacter pylori infection: a dynamic process from diagnosis to treatment. Front. Cell. Infect. Microbiol. 13, 1257817. https://doi.org/10.3389/fcimb.2023.1257817.

van den Berg, F.F., van Dalen, D., Hyoju, S.K., van Santvoort, H.C., Besselink, M.G., Wiersinga, W.J., Zaborina, O., Boermeester, M.A., Alverdy, J., 2021. Western-type diet influences mortality from necrotising pancreatitis and demonstrates a central role for butyrate. Gut 70, 915–927. https://doi.org/10.1136/gutjnl-2019-320430.

Vasudevan, S.O., Behl, B., Rathinam, V.A., 2023. Pyroptosis-induced inflammation and tissue damage. Semin. Immunol. 69, 101781. https://doi.org/10.1016/j.smim.2023.101781.

Wang, G., Liu, Y., Zhou, S.F., Qiu, P., Xu, L., Wen, P., Wen, J., Xiao, X., 2016. Effect of somatostatin, ulinastatin and gabexate on the treatment of severe acute pancreatitis. Am. J. Med. Sci. 351, 506–512. https://doi.org/10.1016/j.amjms.2016.03.013.

Wang, G., Wen, J., Wilbur, R.R., Wen, P., Zhou, S.F., Xiao, X., 2013a. The effect of somatostatin, ulinastatin and Salvia miltiorrhiza on severe acute pancreatitis treatment. Am. J. Med. Sci. 346, 371–376. https://doi.org/10.1097/MAJ.0b013e31827aa2bc.

Wang, L.J., Jin, Y.L., Pei, W.L., Li, J.C., Zhang, R.L., Wang, J.J., Lin, W., 2024. Amuc_1100 pretreatment alleviates acute pancreatitis in a mouse model through regulating gut microbiota and inhibiting inflammatory infiltration. Acta Pharmacol. Sin. 45, 570–580. https://doi.org/10.1038/s41401-023-01186-4.

Wang, R., Yang, F., Wu, H., Wang, Y., Huang, Z., Hu, B., Zhang, M., Tang, C., 2013b. High-dose versus low-dose octreotide in the treatment of acute pancreatitis: a randomized controlled trial. Peptides 40, 57–64. https://doi.org/10.1016/j.peptides.2012.12.018.

Wang, Z., Guo, M., Li, J., Jiang, C., Yang, S., Zheng, S., Li, M., Ai, X., Xu, X., Zhang, W., He, X., Wang, Y., Chen, Y., 2023. Composition and functional profiles of gut microbiota reflect the treatment stage, severity, and etiology of acute pancreatitis. Microbiol. Spectr. 11, e0082923. https://doi.org/10.1128/spectrum.00829-23.

Wu, X.B., Sun, H.Y., Luo, Z.L., Cheng, L., Duan, X.M., Ren, J.D., 2020. Plasma-derived exosomes contribute to pancreatitis-associated lung injury by triggering NLRP3-dependent pyroptosis in alveolar macrophages. Biochim. Biophys. Acta, Mol. Basis Dis. 1866, 165685. https://doi.org/10.1016/j.bbadis.2020.165685.

Xia, H., Guo, J., Shen, J., Jiang, S., Han, S., Li, L., 2023. Butyrate ameliorated the intestinal barrier dysfunction and attenuated acute pancreatitis in mice fed with ketogenic diet. Life Sci. 334, 122188. https://doi.org/10.1016/j.lfs.2023.122188.

Xu, W.F., Wang, Y., Huang, H., Wu, J.W., Che, Y., Ding, C.J., Zhang, Q., Cao, W.L., Cao, L.J., 2022. Octreotide-based therapies effectively protect mice from acute and chronic gastritis. Eur. J. Pharmacol. 928, 174976. https://doi.org/10.1016/j.ejphar.2022.174976.

Yan, X., Lin, T., Zhu, Q., Zhang, Y., Song, Z., Pan, X., 2023. Naringenin protects against acute pancreatitis-associated intestinal injury by inhibiting NLRP3 inflammasome activation via AhR signaling. Front. Pharmacol. 14, 1090261. https://doi.org/10.3389/fphar.2023.1090261.

Yang, J., Wu, B., Sha, X., Lu, H., Pan, L.L., Gu, Y., Dong, X., 2024. Intestinal GSTpi deficiency exacerbates the severity of experimental hyperlipidemic acute pancreatitis. Int. Immunopharmacol. 137, 112363. https://doi.org/10.1016/j.intimp.2024.112363.

Zhang, B., Xue, L., Wu, Z.B., 2024. Structure and function of somatostatin and its receptors in endocrinology. Endocr. Rev. https://doi.org/10.1210/endrev/bnae022.

Zhao, J., Wang, H., Zhang, J., Ou, F., Wang, J., Liu, T., Wu, J., 2022. Disulfiram alleviates acute lung injury and related intestinal mucosal barrier impairment by targeting GSDMD-dependent pyroptosis. J. Inflamm. 19, 17. https://doi.org/10.1186/s12950-022-00313-y.

Zhou, J., Li, M., Chen, Q., Li, X., Chen, L., Dong, Z., Zhu, W., Yang, Y., Liu, Z., Chen, Q., 2022. Programmable probiotics modulate inflammation and gut microbiota for inflammatory bowel disease treatment after effective oral delivery. Nat. Commun. 13, 3432. https://doi.org/10.1038/s41467-022-31171-0.

Zou, M., Yang, Z., Fan, Y., Gong, L., Han, Z., Ji, L., Hu, X., Wu, D., 2022a. Gut microbiota on admission as predictive biomarker for acute necrotizing pancreatitis. Front. Immunol. 13, 988326. https://doi.org/10.3389/fimmu.2022.988326.

Zou, S.F., Peng, Y.H., Zheng, C.M., Fei, Y.X., Zhao, S.W., Sun, H.P., Yang, J.F., 2022b. Octreotide ameliorates hepatic ischemia-reperfusion injury through SNHG12/TAF15-mediated Sirt1 stabilization and YAP1 transcription. Toxicol. Appl. Pharmacol. 442, 115975. https://doi.org/10.1016/j.taap.2022.115975.